Signal propagation and linear response in the delay Vicsek model

Daniel Geiß [1,2] Klaus Kroy [1] and Viktor Holubec [3,*]

[1]*Institute for Theoretical Physics, University of Leipzig, 04103 Leipzig, Germany*
[2]*Max Planck Institute for Mathematics in the Sciences, 04103 Leipzig, Germany*
[3]*Faculty of Mathematics and Physics, Charles University, CZ-180 00 Prague, Czech Republic*

Retardation between sensation and action is an inherent biological trait. Here we study its effect in the Vicsek model, which is a paradigmatic swarm model. We find that (1) a discrete time delay in the orientational interactions diminishes the ability of strongly aligned swarms to follow a leader and, in return, increases their stability against random orientation fluctuations; (2) both longer delays and higher speeds favor ballistic over diffusive spreading of information (orientation) through the swarm; (3) for short delays, the mean change in the total orientation (the order parameter) scales linearly in a small orientational bias of the leaders and inversely in the delay time, while its variance first increases and then saturates with increasing delays; and (4) the linear response breaks down when orientation conservation is broken.

I. INTRODUCTION

Information exchange in animal groups has been suggested to foster survival by improving foraging [1] and predator avoidance [2–6]. The emerging collective behavior is associated with swarm intelligence [7,8] and a collective mind [9]. Indeed, if short-range interactions between group members give rise to scale-free correlations [10–12], this allows for an efficient information propagation through large groups [10,13,14]. And their sensory range is thereby increased way beyond that of its individual members. Inspired by a historical naval battle, where peer-to-peer signaling was employed to spy beyond the horizon, this is sometimes referred to as the Trafalgar effect [15,16]. It is plausible that animal interactions were evolutionary optimized: too low mutual sensitivity might jeopardize a group's cohesion, too high sensitivity could magnify random perturbations into involuntary collective spasms. As examples for advanced collective strategies, previous work has identified leadership [17–20], collective escape waves [21,22], and hierarchical structures [17–20]. From a physical perspective, studies of motile ensembles, ranging from bacterial colonies [23,24] to flocks of birds [22,25], are often subsumed into the field of active matter [26–28]. The associated (active) many-body-theory perspective has already helped to uncover a variety of exotic nonequilibrium collective phenomena [29–33] and hinted at potential technological applications [34–37].

A key ingredient in the interactions of living agents is a time delay between perception and reaction. Signal propagation and processing, as well as actuation suffer from inevitable speed limitations. In general, the associated time delay in the mutual interactions between the agents may enrich the resulting collective dynamics with a hierarchy of instabilities, including oscillations, multistability, and chaos [38–40]. These have been the subject of intense study in the field of dynamical systems [41]. Conversely, delays have also been employed to stabilize unstable orbits in chaotic systems, e.g., via the Pyragas method [42]. In the context of information propagation, time delay has moreover been investigated in connection with sensory [43], social [44] and financial (Bitcoin) [45] networks, as well as in human traffic [46]. For self-propelling particles with retarded pairwise attractions, time delays can trigger behavioral patterns [47,48] reminiscent of dynamical regimes known from (linear) stochastic delay differential equations [38]. Small perception-reaction delays in a Vicsek model (VM) may foster clustering [49] and flocking [50], similarly as in the Cucker-Smale model [51]. In contrast, long delays have the opposite effect [49–51]. From a more technological perspective, time delays naturally play an important role in feedback systems [36,37]. Finally, it was recently suggested that retardation induced by inertia [13,52,53] or by discrete time lags [50] could be the missing link between the VM and the behavior empirically observed in natural swarms [54]. In this respect, it was moreover found that the inertial version of the VM (the so-called inertia spin model) better describes collective turns as observed in natural swarms than the standard VM [55]. However, to the best of our knowledge, there are no other studies of delay effects on the information propagation and response of motile active matter systems.

In the following, we therefore study retarded information spreading and linear response in the two-dimensional delay VM, defined in Sec. II. First, we focus on the ability of an aligned system (flock) to perform collective turns (Sec. III), and its reaction to local perturbations [56] (Sec. IV). For the former case, we study in Sec. V how the signal spreads in space and time and determine the corresponding dispersion relation. In Sec. VI we consider the response of the system to an orientational bias applied to a subgroup of agents

*viktor.holubec@mff.cuni.cz

(so-called leaders) and in particular evaluate the conditions for linearity [57,58]. Finally, Sec. VII summarizes our findings and gives an outlook to possible extensions of the present work.

II. TIME DELAY VICSEK MODEL

The VM [59,60] is a paradigmatic model for dry active matter [28]. Its original version [59] consists of N mobile spins moving with constant speed v_0, and interacting via alignment interactions. We consider the two-dimensional version with time delayed metric interactions [50], where each particle at time $t + 1$ assumes the average orientation of all neighbors at distance less than R at an earlier time $t - \tau < t$, up to some noise. Velocities $\mathbf{v}_i(t)$ and positions $\mathbf{r}_i(t)$ of the individual particles obey the equations of motion

$$\mathbf{v}_i(t+1) = v_0 \mathcal{R}_\eta \left[\mathbf{v}_i(t) + \sum_{j \neq i} n_{ij}(t - \tau) \mathbf{v}_j(t - \tau) \right], \quad (1)$$

$$\mathbf{r}_i(t+1) = \mathbf{r}_i(t) + \mathbf{v}_i(t+1), \quad (2)$$

where the noise operator $\mathcal{R}_\eta \mathbf{v}$ realizes a uniform random rotation by an angle in the range $[-\eta, \eta]$ around its normalized argument $\mathbf{v}/|\mathbf{v}|$. For the chosen metric interactions, the elements of the connectivity matrix n_{ij} are given by $n_{ij}(t) = 1$ if $r_{ij}(t) = |\mathbf{r}_i(t) - \mathbf{r}_j(t)| < R$ and $n_{ij}(t) = 0$ otherwise. We take R as our length unit, i.e., we set $R = 1$, and the time step $\Delta t = 1$ between two consecutive interactions as the time unit. In contrast to the closely related *XY* model [61] the connectivity matrix is time dependent. In the VM with topological interactions, which seems more appropriate for natural bird flocks [62], we expect qualitatively similar results for information spreading as described below [56].

Without a time delay, the model (1)–(2) is just the standard VM [59], which exhibits overdamped orientational dynamics of $\mathbf{v}_i(t)$ [50,54]. At (imposed) high densities, a highly aligned phase emerges, reminiscent of flocking birds. The disordered state found at low densities resembles an insect swarm. For large particle numbers, the transition between these two phases is discontinuous ("first order") [63]. A finite delay time τ [50] or, alternatively, some finite inertia [64] in the dynamical equation for the velocity is known to bring the model predictions closer to the space-time correlations and finite-size scaling observed in natural swarms [54]. Moreover, inertia was argued to stabilize the flock phase and improve the ability of the system to perform collective turns [55]. In the next section, we show that time delay in the interactions, which is often likened to inertia, yields different effects.

III. COLLECTIVE MANEUVER

To sustain their cohesion, flocks need to be able to perform collective maneuvers [55]. We now investigate the ability of individual members to initiate such maneuvers in the delay VM. Specifically, we consider an initially ($t = 0$) fully polarized flock, with all particles moving in the same direction $\mathbf{v}_{\text{init}}/v_0 = (1, 0)^\intercal$, corresponding to the polarization $\Phi = (\sum_i \mathbf{v}_i)^2 / v_0 N = 1$. The initial positions are distributed randomly inside a circle of diameter L_F around the origin. The only exception is a single leader placed at the front of the
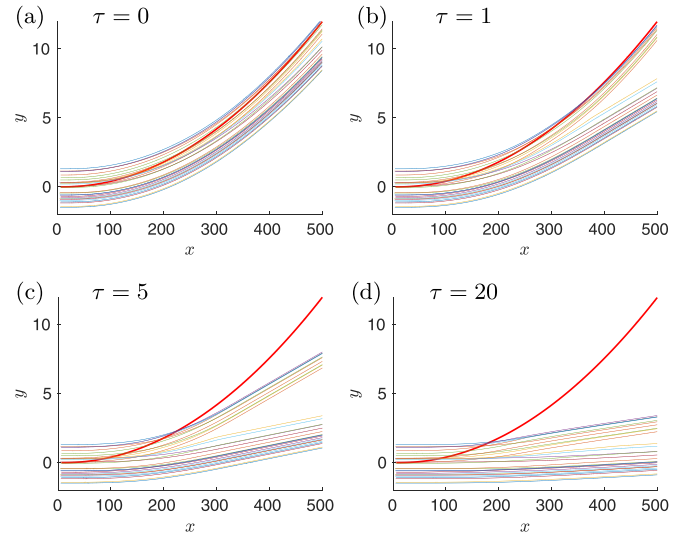

FIG. 1. Fate of a flock in the delay VM. The flock starts with identical initial conditions near the lower left end of each graph and performs 10^3 time steps with four different values of time delay ($\tau = 0, 1, 5, 20$) in the mutual interactions. The bold red line shows the deterministic turn (3) performed by a leader. For $\tau = 0$, the flock partly follows its turn but eventually looses coherence and may even break up. For longer delays, the flock coherence weakens, leading to the delay-induced breaking of the flock. In the limit of very long delay time $\tau \gtrsim L_F/v_0$, the dwell time of the leader in the flock diminishes, and so does its impact on the flock. This is accompanied by a nonmonotonic drop in the total polarization of the flock with increasing τ shown in Fig. 2. Parameters used: $N = 30$, $L_F = 3$, $v_0 = 0.5$, $\varphi = 5 \times 10^{-5}$.

flock, $\mathbf{r}_L(0) = (L_F, 0)^\intercal$. To initialize the particle velocities, we assume that the whole flock had evolved along the x axis according to Eqs. (1) and (2) for $t < 0$, while, for $t \geqslant 0$, the leader is constrained to make a deterministic turn

$$\mathbf{v}_L(t+1) = \mathcal{T}_\varphi \mathbf{v}_L(t). \quad (3)$$

The operator $\mathcal{T}_\varphi$ rotates its argument by an angle φ. Its deterministic time evolution acts as a persistent source of information fed to the flock dynamics. For the sake of clarity, we neglect the noise, $\eta(t) = 0$, for now. Then the only perturbation in the system is the deterministic motion of the leader, and the initially fully polarized flock can be understood as a steady state configuration of the system.

In Fig. 1 we show typical turning events for four different values of the time delay of a small flock of $N = 30$ agents following a slowly turning leader. For short delays, all the particles turn with approximately the same radius, in a manner that is loosely reminiscent of natural bird flocks [13,55,65]. However, due to the accumulating mismatch between the navigation of the flock and its leader, the latter ultimately escapes its followers for arbitrary nonzero turning speeds φ. Its cumulative impact on the overall flock orientation (the order parameter) is determined by its dwell time in the flock. Since the conductive spreading of orientation is diffusive [56] and thus inefficient, the particles that spend most time in the vicinity of the leader follow it more closely than the more remote ones. This leads to a reshuffling of the flock
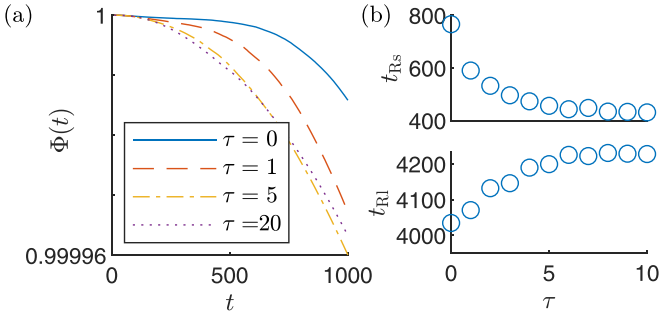
FIG. 2. Time evolution of the polarization for the flocks depicted in Fig. 1, averaged over 100 simulation runs. (a) At short times, the decay of the polarization monotonously speeds up with the delay, reflecting the gradual inability of the flock to follow the leader. At late times, the polarization decays faster for moderate delays than for longer delays (as indicated by the crossing of the yellow dashed line for $\tau = 5$ and the purple dotted line for $\tau = 20$). This is caused by the leader-induced splitting of the flock, which becomes less pronounced with increasing time delay beyond $\tau \gtrsim L_F/v_0$. (b) These two effects are nicely depicted by times t_{Rs} and t_{Rl} measuring the polarization's decay speed at short and asymptotically long times, respectively. Specifically, t_{Rs} is the time when polarization drops to 0.999993 when no splitting events occur for the chosen parameters of the model. t_{Rl} is then defined as time when $\Phi(t_{Rl}) = 0.9993$. We stress that the depicted drop in polarization is a single particle effect caused by the leader leaving the flock of the remaining $N - 1$ agents. The same phenomenology can be observed for arbitrary N. The magnitude of the polarization decays as $1/N$.

formation and an associated defocusing that can eventually rip the flock apart. Interestingly, the effect becomes increasingly pronounced with growing delay τ, but fades again beyond a certain threshold $\tau \gtrsim L_F/v_0$. This nonmonotonicity indicates a trade-off between the delay-induced increase with τ in the time spent in the vicinity of the leader needed for successful alignment, which favors flock break-up, and a correspondingly shortened dwell time of the leader inside the flock, which reduces its cumulative impact. Taking into account noise, one finds that the splitting events become more frequent with increasing noise amplitude. This is expected because randomly turning particles can act as additional "leaders" initiating new splitting events. Similarly, increasing the particle number N for a given v_0 while keeping the initial flock density N/L_F^2 constant eventually always induces splitting of the flock as the information reaching distant parts of the flock during the finite duration of the turn gets strongly damped. On the other hand, increasing the particle number N while keeping the initial flock size L_F constant (thus increasing the initial swarm density) stabilizes the flock (splitting gets less likely) as the relative weight of the individual perturbations decreases. For the same reason, the ability of the flock to follow a single leader decreases with increasing density.

In summary, in the VM, flocks thus only follow slowly turning leaders. Due to the metric interaction rule, better coherence is naturally achieved by more compact flocks. However, no matter the conditions, the leader eventually always leaves a finite flock, as witnessed by the decreasing polarization in Fig. 2. The generally poor take-up of the leader's direction by the VM flocks is a direct consequence

of the averaging interactions, which disperse the information, preventing a perfect alignment. Recent investigations [55] show that in the VM augmented with orientational inertia, the turning information can propagate much more efficiently due to an additional degree of freedom that (approximately) conserves the flock's curvature. As a result, the inertia spin model allows for coherent collective turns where the leader stays inside the flock. Contrary to these findings, the time delay renders the ability of the VM to perform coherent turns even worse. This striking difference between the effects of inertia and delay is interesting because other aspects of the two models, e.g., dynamical critical exponent and shape of time correlation functions, are similar [25,50].

In Sec. VI the turning scenario is revisited from the perspective of the flock's linear response. Before that, we discuss another interpretation of the turning event, in which the "poor obedience" of the flock has a more advantageous connotation.

IV. PERTURBATION

If the leader makes a sudden (or very fast) turn in the scenario of the preceding section, it can be interpreted as a random perturbation in the flock rather than an intended systematic maneuver. In stable systems, such perturbations should not create a strong response. This again reflects the necessity for tuning the information propagation in a flock to an intermediate strength. And, again, delayed interactions can play a role in this respect. Efficient information propagation promotes cohesion and a coherent response of the flock to a stimulus but also tends to make the system overly sensitive to accidental local perturbations that do not qualify as reasonable cues for the whole flock.

To study the response of the delay VM to such "accidental perturbations," we consider the same noiseless scenario as in the preceding section—with the important difference that the leader abruptly turns by an angle φ at time $t = 0$ but subsequently obeys the dynamic equations (1) and (2), rather than following an externally prescribed route. In this case, the system receives information only at time $t = 0$ and relaxes freely, thereafter. The response of the flock in terms of its polarization is plotted in Fig. 3(a), again for four different values of time delay. Two main effects of the time delay on the response can be discerned. First, as already gleaned from the above discussion, delayed interactions cause a lag of the collective response. This increases the relaxation time t_R of the polarization by the delay time τ, i.e., $t_R(\tau) = t_R(0) + \tau$. This ansatz is verified in Fig. 3(c), where we show the relaxation time of the polarization as a function of the delay time. Here the relaxation time t_R is defined as the time when the polarization reaches 99% of its plateau value, i.e., $\Phi(t_R) = 0.99 \Phi(\infty)$. Second, a sufficiently strong retardation of the interactions introduces an oscillatory response in the form of periodic spikes in the polarization dynamics. Their period is given by $\tau + 1$ and their amplitude increases with growing τ and decays with growing laboratory time t. Such delay-induced oscillations are well known to be a hallmark of delay dynamical systems [38,50]. In the delay VM, they can be explained as follows. After the leader has been perturbed, it will spread the perturbation to the rest of the flock but also tend to realign itself with its (former) neighbors. The leader
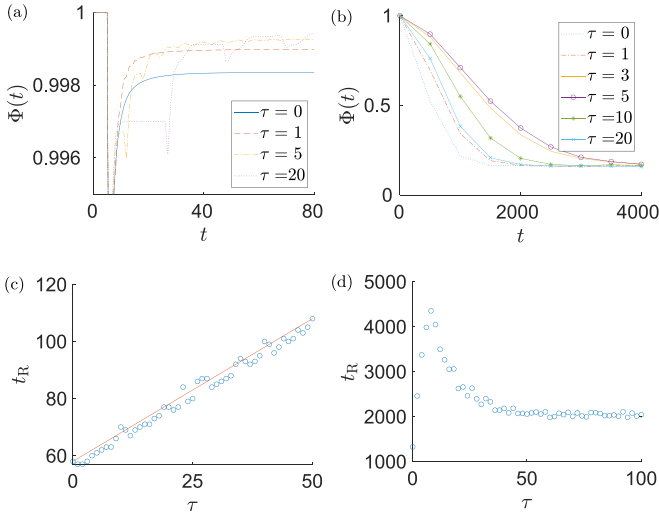
FIG. 3. (a) Relaxation of the flock's polarization after a sudden change of the leader's orientation by the angle $\varphi = 1$ for four different time delays. As in Fig. 2, the depicted effect on flock polarization is caused by a single leader in the $N - 1$ particle flock. Therefore its magnitude decays like $1/N$. (b) Decay of the flock's polarization to its disordered stationary value for strong noise, $\eta = 0.1$. Symbols in panels (c) and (d) show relaxation times corresponding to (a) and (b), respectively, as functions of the time delay. The solid line in (c) depicts the theoretical expectation $t_{\mathrm{R}}(\tau) = t_{\mathrm{R}}(0) + \tau$. Parameters used: $N = 30$, $L_{\mathrm{F}} = 6$, $v_0 = 0.5$, $N_{\mathrm{runs}} = 10^3$.

may therefore already have realigned with the initial direction of its more distant neighbors once these neighbors are affected by the spreading impulse of the initial perturbation. Their delayed reaction may then echo back to the leader, after yet another delay time. This wavelike oscillatory spreading pattern clearly constitutes a pulse propagation. Apart from the crucial delay interaction, it is tied to the finite extent of the perturbing impulse and the subsequent free relaxation of the leader, so that it could not be observed in the turning scenario studied further above, where the leader's dynamics is at all times determined by Eq. (3), which provides a persistent information influx preventing the backlash. However, once the oscillations in the polarization are present, they represent a robust, time-local effect that does not vanish in large ensembles of particles, not even after averaging over the noise [50], unless one introduces sufficient dispersion in the reaction-time delays of the individual particles.

So far, we concentrated on purely deterministic dynamics, for simplicity. But qualitatively similar behavior can also be observed for systems affected by noise. One may think of external noise as consisting of a large ensemble of "accidental perturbations" of the same type as just discussed. They permanently trigger random chains of similar orientational adaptation events as just described, across the whole flock. Let us now consider an initially fully polarized flock whose polarization decays (to zero, if the flock is infinitely large) due to persistent noise. In Fig. 3(b) we show that also in this case the time delay has a stabilizing effect on the system, as it in general increases the polarization decay time. However, the latter does not grow monotonically in τ. Instead, as shown in Fig. 3(d), the decay time t_{R}, defined in the standard way as

$\Phi(t_{\mathrm{R}}) = 1/e$, exhibits a peak for intermediate delays, and then decreases to a finite asymptotic value. We conjecture that this peak results from a competition between the reduced alignment strength and the improved stability against perturbations, caused by the delay. Similar nonmonotonic effects in the delay VM were previously reported in Refs. [49,50].

V. SIGNAL PROPAGATION

Recent studies have investigated the information spreading in the standard VM [56,66,67] and also in the inertia VM [25]. In this vein, we now study how information about the leader's turn propagates through a flock, in the delay VM. In our setting, it is not obvious how to employ the usual information theoretical notions such as entropy or channel capacity [68,69]. Therefore, our analysis relies on the concept of maximum response [56] or, more generally, maximum correlation [25].

The change of state of a Vicsek flock is described by the accelerations $\mathbf{a}_i(t) = \dot{\mathbf{v}}_i(t)$ or, equivalently, by changes $\dot{\theta}(t)$ of the orientations $\theta_i(t) = \arctan[v_{y,i}(t)/v_{x,i}(t)]$ of the individual particles. Following Ref. [56], we take the turning rate $\dot{\theta}(t)$ as a measure for the strength of the signal arriving at the particle i at time t. For our specific setup, this approach is equivalent to the acceleration-correlation-based approach applied in Refs. [25,70]. Similarly as in Sec. III, we consider in this section an initially highly polarized flock with $\theta_i(0) = 0$ and a leader performing a deterministic turn. However, in contrast to the above scenarios we assume that the leader changes its orientation instantaneously at time $t = 0$ by an angle φ that remains fixed thereafter. In this setting, the signal source is better localized in space and time than in the case of the continuous turn of Sec. III. To minimize boundary effects, we also initialize the leader in the center of the flock instead of its front, and we neglect the noise. For a nonvanishing noise, the system becomes unstable unless it is confined by boundary conditions.

A. Spatial propagation of a signal

Let us first discuss the signal spreading through the flock of immobile ($v_0 = 0$) agents with a static interaction network. In this case the distance to the source of the signal is a well defined quantity and thus we can take the corresponding results as a standard for further analysis. Besides, since the lattice is fixed, the information spreads homogeneously and solely by conduction [56]. For a thorough analysis of this scenario for the standard VM ($\tau = 0$), see Ref. [56].

In Fig. 4 we show the resulting orientations, $\theta_i(t)$, and their rates of change $\dot{\theta}_i(t)$, as functions of the distance d_i from the leader for $\tau = 0$ and $\tau = 1$. To avoid a dependence on the initial condition, the shown values are averaged with respect to N_{runs} simulation runs as follows. We first collect all data $\{d_i, \theta_i(t), \dot{\theta}_i(t)\}_{i=1,...,N}$ from the individual simulations runs and sort the total data with respect to the distance d_i. The so obtained ordered sets of NN_{runs} data points are then smoothed by calculating a sliding average over N_{runs} neighboring data points. The corresponding averages are denoted by the symbol $\langle \bullet \rangle_{nn}$.
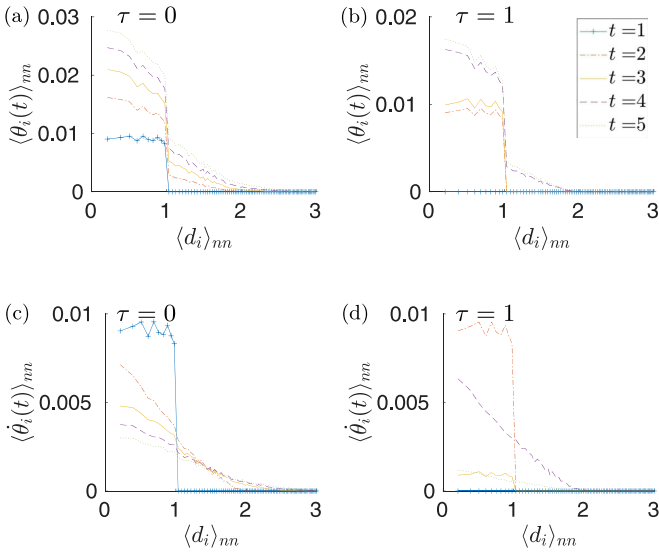
FIG. 4. Time evolution of the average orientation $\theta_i(t)$ (a), (b) and its rate of change $\dot{\theta}_i(t)$ (c), (d) for a stationary flock with $v_0 = 0$ and $\tau = 0, 1$. The signal induced by a leader at the origin spreads in steps of the size of the interaction radius $R = 1$. Delay induces oscillations of $\dot{\theta}_i(t)$ with the period $\tau + 1$. Parameters used: $N = 1000$, $L_F = 20$, $\varphi = 0.1$, and $N_{\text{runs}} = 10^2$.
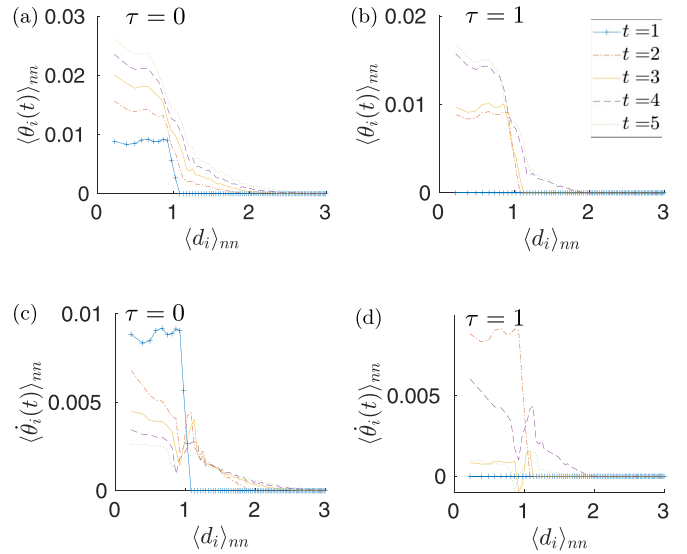
FIG. 5. Time evolution of the average orientation $\theta_i(t)$ (a), (c) and its rate of change $\dot{\theta}_i(t)$ (b), (d) for a moving flock with $v_0 = 0.5$ and $\tau = 0, 1$. Due to the breaking of the rotational symmetry of the static network (Fig. 4), the spreading is enhanced in the direction of the leader's motion. This results in a kink in $\dot{\theta}_i(t)$ at $d_i = R$. Other parameters are the same as in Fig. 4.

Figures 4(a) and 4(c) show that, for $\tau = 0$, the information spreads in "steps" of the width of one interaction radius $R = 1$. After the first time step, the information is homogeneously distributed within the interaction radius $R = 1$ because the corresponding particles interacted equally with the localized information source. The rates $\dot{\theta}_i(t)$ monotonically decrease with the distance from the leader, because particles closer to the leader interact with more neighbors that have already changed their orientation. For time delay $\tau = 1$, the information in Fig. 4(b) starts spreading only at time $t = \tau + 1 = 2$. Furthermore, temporal oscillations of period $\tau + 1$ are induced in $\dot{\theta}_i(t)$, for the same reasons as explained above. In Fig. 4(d) these oscillations manifest themselves as a large $\dot{\theta}_i(t)$ at times $t = 2$ and 4 and a strongly damped $\dot{\theta}_i(t)$ at times $t = 1, 3$, and 5. Regardless of the time delay, the orientations $\theta_i(t)$ exhibit a discontinuity for $d_i = R$ that increases with time, as a result of the continuous influx of information from the fixed leader.

For moving flocks with $v_0 > 0$, the distance traveled by the signal is no longer unambiguously defined. Even though it might seem inadequate, one possible choice of d_i is still the distance to the leader at time $t = 0$ as it gives qualitatively the same results as other definitions, e.g., one that is based on a comoving frame [56]. In what follows, we thus stick to this definition. In Fig. 5 we report again the orientations, $\theta_i(t)$ and their rates of change $\dot{\theta}_i(t)$, as functions of the (initial) distance d_i to the leader. The resulting curves are similar to those for the static network, as shown in Fig. 4. However, the discontinuity in $\theta_i(t)$ at the interaction range, $d_i = R$, is now smeared out and the rate $\dot{\theta}_i(t)$ exhibits concomitant kinks. Both effects result from the anisotropy of the "convective" signal propagation caused by the motion of the leader. For $v_0 > 0$, both the leader and its "interaction zone" move. This affects differently particles in the direction of the leader than

those in the opposite direction, which we do not distinguish when evaluating the shown results. The downward kink in $\dot{\theta}_i(t)$ corresponds to the neighbors behind the leader, which leave its interaction zone, and the upward kink corresponds to the particles in front, entering its interaction zone. Averaging these two effects then induces the smearing of the discontinuity of the orientation $\theta_i(t)$ as a function of distance, at the edge of the interaction zone.

B. Dispersion relation

A central quantity in the study of signal propagation is the signal speed, or, equivalently, the dispersion relation. However, to define these quantities for the VM is neither trivial nor unique. Consider the typical time evolution of the signal strength, measured in terms of $\dot{\theta}_i(t)$. As shown in Fig. 6(a), the signal intensity $\dot{\theta}_i(t)$ reaching an agent i at some time $t > 0$ is initially very low and grows over time until it reaches a maximum and starts to decay. For a stationary or slowly moving flock, for which the information spreading is dominated by conduction, the time when the signal first reaches a particle at distance d_i from its source can roughly be estimated as d_i/R. This is the time required for the signal to arrive from the leader's initial position, if traveling along the shortest path. This initial signal gets diluted by a factor $1/N_{\text{int}}$ after each time step, since it is distributed among the $N_{\text{int}} \approx NR^2/L_F^2$ nearest neighbors, on average. This explains why it becomes very weak at its spreading front. As the number of possible paths connecting the initial position of the leader with the nearby particles in the flock increases over time, also their perceived signal intensity, as well as the rate of change $\dot{\theta}_i(t)$ of their orientation, grows. Once the particles thereby become increasingly aligned with the leader, $\dot{\theta}_i(t)$ decays again. In what follows, we identify the time when $\dot{\theta}_i(t)$ reaches its
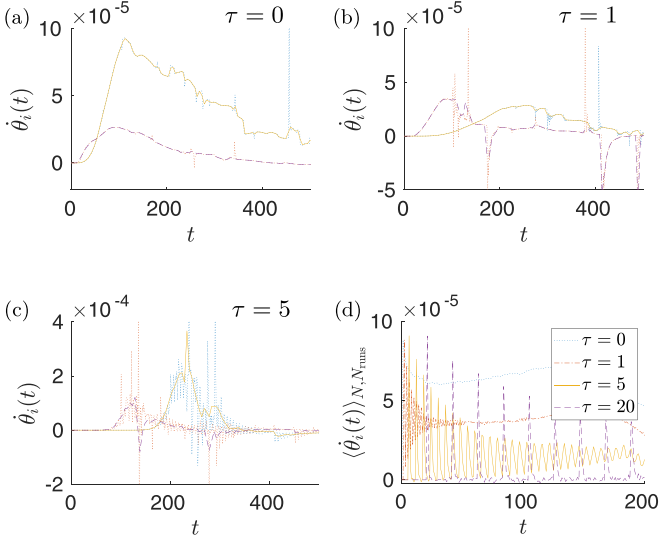
FIG. 6. (a)–(c) Time evolution of the signal intensity $\dot{\theta}(t)$, as perceived at two different particles, bare (blue and red dotted lines) and smoothed (solid yellow and dashed purple lines) versions, for $\tau = 0, 1, 5$, and (d) averaged over all N particles and N_{runs} simulation runs. Parameters used: $N = 10^3$, $L_F = 20$, $v_0 = 0.5$, $\varphi = 0.1$.
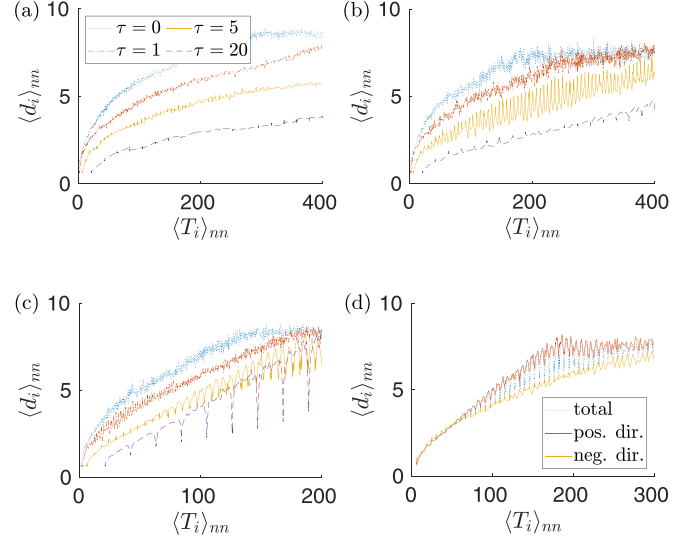

FIG. 7. (a)–(c) The dispersion relations obtained as the average distance from the leader d_i at time T_i when the change of the orientation $\dot{\theta}_i(t)$ peaks for $v_0 = 0$ (a), $v_0 = 0.1$ (b), and $v_0 = 0.5$ (c). With increasing time delay, the signal spreads slower and the dispersion relation becomes a linear curve overlaid by oscillations. (d) The direction-resolved dispersion relations for agents in the upper (positive direction, red line) and the lower (negative direction, yellow line) half-plane for $v_0 = 0.5$ and $\tau = 5$. The corresponding overall dispersion relation (total, blue line) oscillates between the direction-resolved dispersion relations. Parameters used: $N = 10^3$, $L_F = 20$, $\varphi = 0.1$, $N_{\text{runs}} = 10^2$.

maximum as the (characteristic) signal propagation time T_i. The corresponding signal speed is d_i/T_i. For more details concerning this choice, see Ref. [56].

To inspect the signal propagation more closely, consider the time evolution of the signal strength at two given particles, as depicted in Figs. 6(a)–6(c). Each of the three panels corresponds to a different value of the delay. The most striking feature of the raw data (dotted blue and red curves) is the presence of sharp spikes, which become more frequent for long time delays. We reckon that these "resonances" are due to random inhomogeneities in the initial conditions. At a first glance, identifying the time T_i with these spikes might be feared to lead to erroneous estimates for the signal speed. Therefore, we alternatively considered the smoothed profiles depicted by the solid yellow and dashed purple lines. They were obtained by first performing sliding averages over five raw data points and then substituting the remaining outliers (beyond five times the average $\langle \dot{\theta}_i(t) \rangle_t$ over the shown time interval) with an average value of their neighboring points. But the results for the dispersion relations remained qualitatively the same.

Besides the spurious spikes, the curves for time delays $\tau > 0$ again exhibit oscillations, which can even reach negative values as the particle orientations tend to align to their previous values. The period of these oscillations is $\tau + 1$ and their magnitude increases with growing delay. For sufficiently long delays, the signal strength exhibits sharp positive and negative peaks as the particle is either aligned with its own initial orientation or with the initial direction of the leader. These sharp peaks are even better visible in Fig. 6(d), where we show the average of $\langle \dot{\theta}_i(t) \rangle_{N,N_{\text{runs}}}$ taken over all N particles and N_{runs} simulation runs, for the same values of time delay as in Figs. 6(a)–6(c). This quantity measures the total rotation rate in the flock at the given time. For short delays, the signal

is initially stronger, but the envelopes of the peaks induced by long delays have the longer decay time.

In Figs. 7(a)–7(c) we show the main results of this section, which are the dispersion relations for different speeds v_0 and time delays τ. They were obtained as follows. We evaluated the times T_i for the maximum signal strength $\dot{\theta}_i(t)$ for all NN_{runs} particles in all N_{runs} simulation runs. Then, we calculated the distances $d_i(T_i)$ from the leader at time $t = 0$ to particle i. Finally, we averaged the values obtained for the individual particles over N_{runs} nearest neighbors (the $\langle \bullet \rangle_{nn}$ average introduced in Sec. V). The relation of both averages is shown in the plot.

For distances $d_i \approx L_F/2 = 10$ near the boundary of the flock, the dispersion relations are strongly affected by boundary effects, leading to a "flattening" of the curves. For all considered speeds, a retardation of the interactions slows the signal propagation through the system. In accord with Ref. [56], the dispersion relations are diffusive ($\langle d_i \rangle_{nn} \sim \sqrt{\langle T_i \rangle_{nn}}$) for $\tau = 0$ and small speeds v_0. For a positive v_0, increasing τ leads to gradually more linear dispersion relations with slopes of the order of the leader's speed $v_0 \sin \varphi$ relative to the rest of the flock. Specifically, for $v_0 = 0.1$ and $\varphi = 0.1$ we have $v_0 \sin \varphi \approx 0.01$, and we find the slope 0.01 for $\tau = 5$ and $\tau = 20$. For $v_0 = 0.5$ also the dispersion relation for $\tau = 0$ has a significant linear part. The slopes corresponding to all measured dispersion relations for this velocity are approximately 0.4, while $v_0 \sin \varphi \approx 0.5$. The agreement between the velocity of the leader relative to the rest of the flock and the slopes of the dispersion relations strongly suggests that the

spreading of information is, in these regimes, predominantly due to the convective transport caused by the motion of the leader and not due to the conductive transport effected by the interparticle interactions within the flock.

For longer delay times, the dispersion relations exhibit downward spikes periodically occurring with the period $\tau + 1$, an overall linear increase of the upper envelope, and a diffusive increase in the lower envelope. In Fig. 7(d) we show that the dispersion relations roughly oscillate between the values attained for specific spreading directions of the signal with respect to the leader. To demonstrate this, we display dispersion relations calculated from the part of the flock in the upper (positive) and lower (negative) half-planes. For the chosen turning angle $\varphi = 0.1$, the leader moves toward the former and away from the latter. In accord with the findings of Ref. [56], the dispersion relation for the positive direction is, for large enough speed, linear, while the dispersion relation for the negative direction remains diffusive, regardless of v_0 and τ. One can thus conclude that introducing the time delay induces some filtering out of the conductive component of the dispersion relation (the weight given to the conductive component corresponds to the periodically occurring spikes, which involve only a few data points compared to the regions between them, corresponding to the convective spreading). Besides, it was found in Ref. [50] that increasing the time delay for a nonzero speed v_0 increases the effective speed of the individual agents. As the convective component of the dispersion relation becomes more pronounced with increasing speed, these two effects make the dispersion relation gradually more convective with increasing time delay (except for the spikes).

Using a simplified spin-wave theory for the (continuous-time) VM, valid for small perturbations around a common direction of the whole flock, the dispersion relation for the delay VM can be obtained analytically. The linearized model is derived, e.g., in the Supplementary Information of Ref. [50]. It reads

$$\tilde{\eta}\dot{\varphi}(\mathbf{r}, t) = Jn_c a^2 \triangle\varphi(\mathbf{r}, t - \tau) + Jn_c[\varphi(\mathbf{r}, t - \tau) - \varphi(\mathbf{r}, t)]$$
$$+ \sqrt{2Da^3}\xi(\mathbf{r}, t), \quad (4)$$

where $\varphi(\mathbf{r}, t)$ describes fluctuations in orientation of the individual particles. The positive parameters J and n_c determine the strength of the interparticle interactions, $a > 0$ denotes a typical interparticle distance, $\tilde{\eta} > 0$ sets the intrinsic relaxation timescale, and D determines the amplitude of the Gaussian white noise $\xi(\mathbf{r}, t)$. The corresponding dispersion relation can be determined after neglecting the noise and taking the Fourier transform of the linearized dynamical equation in space and time [25]. Denoting the Fourier variables corresponding to space and time as ω and k, respectively, and assuming just one spatial dimension, we obtain the transcendental equation

$$\tilde{\eta}\omega = -iJn_c[(k^2a^2 - 1)\exp(i\omega\tau) + 1]. \quad (5)$$

For $\tau = 0$, it yields the purely imaginary dispersion relation $\omega(\mathbf{k}) = -iJn_c a^2 k^2$, describing an exponentially damped diffusive transport. For a nonzero delay,

$$\omega(\mathbf{k}) = \frac{i}{\tau}\{-\tilde{J} + W_n[(1 - a^2k^2)\tilde{J}\exp(\tilde{J})]\}, \quad (6)$$

$n = 0, \pm 1, \pm 2, \ldots$, where $W_n(.)$ is the nth branch of the Lambert W function, which is a multivalued function frequently entering solutions to time-delay systems [38], and $\tilde{J} = Jn_c\tau/\tilde{\eta}$. For $n \neq 0$ the dispersion relation has nonzero real components which correspond to a damped a wavelike (ballistic) transport [25]. Unfortunately, all these insights still do not provide a fully satisfactory intuitive explanation of the form of the dispersion relation observed in our simulations. Gaining such an intuition will thus require additional efforts.

To put these results into a broader context, we note that, from the point of view of natural systems, the spikes may be considered an artifact of choosing precisely the same delay time for all interactions. In practical applications, the time delay is more likely to be randomly distributed among the individuals, so that the spikes are expected to average out, at least to some extent. With this in mind, the robust conclusion is that the retarded interactions embodied in the delay VM induce linear dispersion relations, similarly as to what inertia does in a generalized VM with underdamped orientations [25]. In the underdamped variant of the VM, the dispersion relation can be derived analytically [71] and the ballistic/convective transport can be intuitively explained as a result of an additional (approximately) conserved degree of freedom [25].

VI. LINEAR RESPONSE TO A LEADER

So far we have analyzed the response of a Vicsek flock with retarded interactions in terms of signal propagation, as appropriate in the most general context of its applications. However, in a more physics-focused context, it may be more natural to interpret the results within the framework of linear response theory. Close to equilibrium, noninvasive measurements of equilibrium correlation functions suffice to know the response functions for arbitrary weak perturbations [72]. For systems far from equilibrium, like the VM, such practical relations are generally unavailable [73–76]. Nonetheless, once the response coefficients for a specific perturbation are determined, the resulting phenomenological law still provides a valuable description of the system's response to that perturbation.

In accord with our previous discussion, we will investigate the response of the delay VM to perturbations induced by a (or various) leader(s). To provide results independent of initial conditions, we consider perturbations that bring the system from one steady state to another perturbed one. The VM eventually converges to a steady state, which is independent of the initial conditions, for a nonzero rotational noise and if the model is solved, e.g., with periodic boundaries. The collective maneuver scenario of Sec. III requires that the size of the periodic box is inversely proportional to the curvature of the leaders' trajectory (so that it fits in the box), which is not a suitable situation for computer analysis. On the other hand, the perturbation scenario of Sec. IV induces a relaxation of the system to its (slightly rotated) initial steady state, and one can measure the characteristics of this relaxation, which have to some extent been discussed in Sec. IV. We now turn to the scenario of Ref. [58], where one applies a permanent torque to the leader(s), which induces a steady state with a nonzero circular flux of the particles.
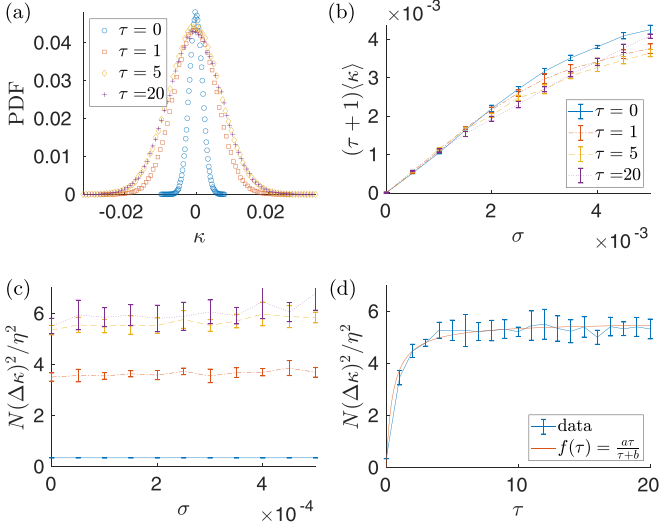
FIG. 8. (a) The probability distribution of the curvature (8) for vanishing bias, $\sigma = 0$. (b) Average curvature as function of σ for four delay times. (c) Corresponding variance. (d) Variance of curvature as function delay time (symbols with error bars) and the empirical fit $a\tau/(\tau + b)$ with parameters $a = 5.57$ and $b = 0.5$ (solid line). Parameters used: $N = 10^3$, $N_{\rm L} = 0.05N$, $\rho_0 = 4$, $v_0 = 0.5$, and $\eta = 0.1$.

Specifically, we consider a system of N particles inside a square box with sides of length L and periodic boundary conditions. We again assume that the individual particles except for the leader obey Eqs. (1) and (2). However, different from the previous section, we consider a small but nonzero value of the noise η, such that the unperturbed system eventually reaches a highly ordered (yet noisy) nonequilibrium steady state. We initialize the system at time $t = 0$ in a polarized state, let it evolve until time t_I when it reaches a steady state independent of the initial data, and then switch on a perturbation affecting $N_{\rm L}$ randomly chosen leaders. Specifically, we assume that velocities of the leaders obey the form

$$\mathbf{v}_{\rm L}(t+1) = v_0 \mathcal{T}_\varphi \mathcal{R}_\eta \left[\mathbf{v}_{\rm L}(t) + \sum_{j \neq i} n_{ij}(t-\tau) \mathbf{v}_j(t-\tau) \right],$$
(7)

where the operator $\mathcal{T}_\varphi$ applies a deterministic rotation by an angle φ to its argument. Following Ref. [58], we study how this perturbation affects the discrete curvature in the overall velocity, defined as

$$\kappa(t) = \bar{\mathbf{\Phi}}(t-1) \times \bar{\mathbf{\Phi}}(t),$$
(8)

where $\bar{\mathbf{\Phi}}(t) = 1/(Nv_0) \sum_i \boldsymbol{v}_i(t)$ denotes the mean orientation of the flock at time t. The resulting dependence of the average curvature $\langle\kappa\rangle$ on the (relative) strength $\sigma \equiv \varphi N_L/N$ of the perturbation is depicted in Fig. 8. In this section, averages $\langle\kappa\rangle \equiv \lim_{t_I \to \infty} t^{-1} \int_{t_I}^{t_I+t} dt' \kappa(t')$ are calculated over time after the system reached the steady state, with $t = 2 \times 10^4$ and $t_I = 10^4$. The shown error bars correspond to standard deviations of these averages computed from 10 independent realizations of the numerical experiment.

Figure 8(a) illustrates that, for $\sigma = 0$, the flock turns randomly and $\kappa(t)$ is a Gaussian random variable with zero mean, $\langle\kappa\rangle = 0$. Imposing a small directional bias $\sigma \ll \eta$ to the leaders induces an overall nonzero mean curvature,

$$\langle\kappa\rangle = \alpha\sigma,$$
(9)

which increases linearly with σ [see Fig. 8(b)]. On the other hand, the variance, $(\Delta\kappa)^2 \equiv \langle\kappa^2\rangle - \langle\kappa\rangle^2$, in Fig. 8(c) remains constant. For our case of highly aligned flocks (small enough η and large enough density N/L^2), the slope α is approximately given by $(1 + \tau)^{-1}$. Notice how the individual curves in Fig. 8(b) depart from the initially common straight line. The linear-response regime is diminished for both long time delays and large directional biases, and the expression for α holds the better the smaller the product $\sigma\tau$. The dependence of the variance on the time delay saturates. Its functional form is well parametrized by $\Delta\kappa^2 \approx a\tau/(\tau + b)$ [see Fig. 8(d)]. Furthermore, for dense flocks, the variance increases with the noise as $(\Delta\kappa)^2 \propto \eta^2$, independent of the perturbation σ (for the corresponding illustrations, see Ref. [58]).

In the Appendix we show how this behavior can be understood analytically, based on a simplified model. Here we provide the emerging intuitive explanation. For vanishing delay and in two dimensions, the curvature (8) can be rewritten as $\kappa(t) = \sin\langle\Delta\theta\rangle_N$ with $\langle\Delta\theta\rangle_N = N^{-1}\sum_i[\theta_i(t) - \theta_i(t-1)]$ denoting the mean change of orientation during one time step. For small perturbations φ, $\langle\Delta\theta\rangle_N \ll 1$ and thus $\kappa \approx \langle\Delta\theta\rangle_N$. For weak noise, high average density, and vanishing delay, the local density of the VM is approximately homogeneous [64]. As a result, the total orientation (or information) $N^{-1}\sum_i \theta_i(t)$ is for $\varphi = 0$ approximately conserved [56]. For $\varphi > 0$, it is then reasonable to assume that the change in the total orientation is directly given by the directional bias applied to the leaders, i.e., $\langle\Delta\theta\rangle_N = 1/N\sum_1^{N_L} \varphi = \sigma$. For a nonzero delay, the orientational change is stretched out over $\tau + 1$ time steps, reducing $\langle\Delta\theta\rangle_N$ by the factor $\tau + 1$. Figure 8(b) can thus be regarded as a verification of the (approximate) information conservation in a highly ordered Vicsek flock. Large biases φ can break the highly ordered state and introduce growing density fluctuations which cause the breakdown of orientation conservation [56] and, as a consequence, linear response. Similarly, as we have demonstrated above, long delays tend to decouple the leaders from their neighborhoods, which also induces fluctuations in density, with the same consequences.

In this vein, the variance of the curvature can be approximated as

$$\Delta(\kappa)^2 = \Delta\left(\frac{1}{N}\sum_i \kappa_i\right)^2 = \frac{1}{N}\Delta(\kappa_i)^2,$$
(10)

where $\kappa_i = \Delta\theta_i$. To expand the square, we assumed that the orientational fluctuations $\Delta\theta_i$ of individual agents are statistically independent, which is sensible for small perturbations φ of a highly aligned state. Assuming that the fluctuations are caused solely by the noise, we get $\langle\Delta\theta_i^2\rangle \approx \int_{-\eta}^{\eta} \tilde{\eta}^2 \, d\tilde{\eta}/(2\eta) = \eta^2/3$. Altogether, we thus find the variance $\Delta(\kappa)^2 \propto \eta^2/N$, which explains the findings in Ref. [58]. According to our argument, this scaling should be a direct consequence of the law of large numbers. Introducing a finite delay enhances effects of the noise on the dynamics and triggers oscillations [38].

As a result, the curvature variance strongly increases with the delay. Unfortunately we were not able to rationalize the observed quantitative dependence of the variance on the time delay, shown in Fig. 8(d), from the equations of motion.

VII. CONCLUSION AND OUTLOOK

In summary, we have studied the response to orientation perturbations in the two-dimensional delay Vicsek model. We have found that a time delay diminishes the ability of strongly aligned systems to follow a leader moving along a predetermined path (different from what has been reported for inertia [55]) and increases the stability of these systems against sudden local fluctuations of orientation. Both effects are caused by the decreased information (orientation) propagation through the system and the stretched time-correlations in the system, due to the delay. Their combination explains the findings in Refs. [49,50] that short delays facilitate and long delays hinder flocking in the delay VM.

In the scenario of a sudden turning pulse applied to a leader, the source of information or perturbation is well localized in space and time. Inspired by [25], we used the induced orientational acceleration as a measure for the signal strength to study the propagation of information (orientation) through the system. As typical for delay systems [38], a time delay causes oscillations. In the present context, they are manifestly seen in the orientational accelerations. Their amplitude, period, and decay time (and thus system memory) all increase with growing delay [50]. To measure the speed of information propagation through the system, we used the maximum of the acceleration pulse transmitted through the flock. We found that the dispersion relation for the signal spreading is diffusive (the distance traveled by the signal ∝ square root of the traveled time) for small speeds and short time delays, but becomes increasingly ballistic (linear) for long delays and high speeds.

We have finally investigated the linear response of highly ordered systems to a weak orientational bias, applied to a subgroup of agents (leaders). We found that the overall change of the flock's orientation is a linear function of the perturbation for short enough time delays and weak enough orientational biases. The linear response regime coincides with the regime of low density fluctuations, where the total information (or average orientation) of the flock is (approximately) conserved. Furthermore, we provided intuitive and analytical arguments for the observed functional dependencies of the mean total orientational change and the corresponding variance.

While our work provides a first understanding of retardation effects in active many-body dynamics, it also raises some further questions. The choice of a universal value of the discrete time delay for all members of the flock certainly oversimplifies the conditions prevailing in natural flocks and swarms, and it would be desirable to get a better understanding of the concomitant internal averaging and its role in suppressing the oscillatory instabilities observed in our idealized model. Also, the reaction capabilities of natural agents will usually be described by more complicated memory functions [38,77]. Further, it could be interesting to investigate more thoroughly the effects of time delay on the collective memory of the flock, which is an important ingredient

in the understanding of so-called swarm intelligence [7,34]. Our present results confirm the natural expectation that the system's relaxation time is sensitive to the delay time. Another direction could be to study information spreading in more complex interaction networks, e.g., with distributed individual weights for the flock members. Such leadership hierarchies are often observed in natural groups [17,18], and it has been argued that they increase the group fitness [18–20]. For instance, it is known that a few (well-connected) agents, known as superspreaders, lead to a rapid increase in disease (or fad) spreading in epidemiology [78–80].

APPENDIX: EXACTLY SOLVABLE MODEL

The dependence of the first two moments of the mean curvature (8) on the delay time τ, discussed in Sec. VI, can be obtained using a simple mean-field model. Consider a system of N mutually interacting particles with a single leader (index L) that interacts with the average flock orientation $\theta_0(t)$ of the other $N - 1$ flock members. The orientations obey the dynamical equations

$$\theta_{\mathrm{L}}(t+1) = \frac{1}{N}[\theta_{\mathrm{L}}(t) + (N-1)\theta_0(t-\tau)] + \varphi + \xi_{\mathrm{L}}(t), \tag{A1}$$

$$\theta_0(t+1) = \frac{1}{N}[\theta_0(t) + (N-2)\theta_0(t-\tau) + \theta_{\mathrm{L}}(t-\tau)] + \xi_0(t). \tag{A2}$$

The symbols $\xi_{\mathrm{L}}(t)$ and $\xi_0(t)$ denote independent δ-correlated angular noises uniformly distributed within the interval $[-\eta, \eta]$. The mean orientation of the system, $O(t) \equiv \langle \theta_i(t) \rangle_N = [\theta_{\mathrm{L}}(t) + (N-1)\theta_0(t)]/N$, obeys the equation

$$O(t+1) = \frac{1}{N}[O(t) + (N-1)O(t-\tau)] + \sigma + \hat{\xi}(t) \tag{A3}$$

with $\sigma = \varphi/N$. The noise $\hat{\xi}(t) = [\xi_{\mathrm{L}}(t) + (N-1)\xi_0(t)]/N$ has variance $\langle \hat{\xi}^2 \rangle = (N^2 - 2N + 2)\eta^2/(3N^2)$.

The difference equation (A3) for the column vector $\boldsymbol{O}(t) \equiv (O(t), \ldots, O(t-\tau))^{\mathsf{T}}$ can be solved using its matrix representation,

$$\boldsymbol{O}(t+1) = M\boldsymbol{O}(t) + \boldsymbol{\sigma} + \hat{\boldsymbol{\xi}}(t). \tag{A4}$$

Here $\boldsymbol{\sigma} \equiv (\sigma, 0, \ldots, 0)^{\mathsf{T}}$ and $\hat{\boldsymbol{\xi}}(t) \equiv (\hat{\xi}(t), 0, \ldots, 0)^{\mathsf{T}}$ are column vectors of length $\tau + 1$, and M is a $(\tau + 1) \times (\tau + 1)$

square matrix with all elements equal to zero except for $M_{11} = 1/N$, $M_{1(\tau+1)} = (N-1)/N$, and $M_{(i+1)i} = 1$, $i = 1, \ldots, \tau$. The formal solution to this equation is

$$\boldsymbol{O}(t) = M^t \boldsymbol{O}(0) + \sum_{i=0}^{t-1} M^i [\boldsymbol{\sigma} + \hat{\boldsymbol{\xi}}(t-i-1)], \qquad (A5)$$

where $\boldsymbol{O}(0)$ is the initial condition, which we set to 0 (all particles aligned with the x axis). Our goal is to calculate the change $\kappa(t) = O(t) - O(t-1)$ of the mean orientation. The corresponding vector $\boldsymbol{\kappa}(t) = (\kappa(t), \ldots, \kappa(t-\tau))^\mathsf{T}$ is given by $\boldsymbol{O}(t) - \boldsymbol{O}(t-1)$ and reads

$$\boldsymbol{\kappa}(t) = M^{t-1} [\boldsymbol{\sigma} + \hat{\boldsymbol{\xi}}(0)] + \sum_{i=0}^{t-2} M^i [\hat{\boldsymbol{\xi}}(t-i-1) - \hat{\boldsymbol{\xi}}(t-i-2)]. \qquad (A6)$$

At late times, $\kappa(t)$ reaches a steady state, in which all elements of the vector $\boldsymbol{\kappa}(t)$ have the same mean and variance, given by $\langle \kappa \rangle$ and $\langle \Delta \kappa^2 \rangle$. Specifically, we find

$$\langle \boldsymbol{\kappa} \rangle = M_\infty \boldsymbol{\sigma}, \qquad (A7)$$

$$\langle \kappa^2 \rangle - \langle \kappa \rangle^2 = \langle \hat{\xi}^2 \rangle R_{11}, \qquad (A8)$$

where $M_\infty \equiv \lim_{t \to \infty} M^t$, $R = M_\infty^\mathsf{T} M_\infty + 2S - M_\infty^\mathsf{T} S - S M_\infty$, and $S \equiv \sum_{i=0}^{\infty} (M^i)^\mathsf{T} M^i$. The right-hand side of Eq. (A8) results from multiplying the sum in Eq. (A6) by itself and using the Markov condition $\langle \hat{\xi}(t) \hat{\xi}(t') \rangle = \langle \hat{\xi}^2 \rangle \delta_{tt'}$ for the stationary noise correlation function.

It is straightforward to verify, e.g., by calculating left and right eigenvectors corresponding to the eigenvalue 1, that the
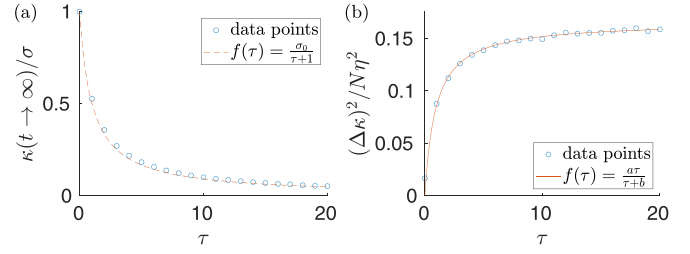

FIG. 9. Noise-averaged stationary orientational change. Symbols depict the mean (a) and variance (b) as functions of the delay time. The dashed line in (a) is the analytical prediction (A9), and the dashed line in (b) is the empirical fit $a\tau/(\tau + b)$ with parameters $a = 0.17$ and $b = 0.93$.

stationary matrix M_∞ has all elements in its first column equal to $c(N-1)/N$, with $c = [(N-1)/N + \tau]^{-1}$. Its remaining elements are equal to c. Hence, we find that all elements of $\langle \boldsymbol{\kappa} \rangle$ are given by σc, and thus, in agreement with the discussion in Sec. VI,

$$\langle \kappa \rangle = \frac{\sigma}{(N-1)/N + \tau}. \qquad (A9)$$

In Fig. 9(a) we show agreement of this prediction with a numerical solution to Eqs. (A1) and (A2).

Equation (A8) is a scalar product of two identical vectors of length $(\tau + 1)$ containing in all entries the variance $(\Delta\kappa)^2$. Thus we find

$$(\Delta\kappa)^2 = \frac{N^2 - 2N + 2}{N^2} \frac{\eta^2}{3(\tau+1)} R_{11}. \qquad (A10)$$

While we were not able to extract the τ and N dependence of the matrix element R_{11} analytically, Fig. 9(b) shows that the τ dependence of the calculated $(\kappa)^2$ is well described by the empirical formula $a\tau/(\tau + b)$, already employed in Sec. VI.

[1] T. Pitcher, A. Magurran, and I. Winfield, Fish in larger shoals find food faster, Behav. Ecol. Sociobiol. **10**, 149 (1982).

[2] S. Neill and J. M. Cullen, Experiments on whether schooling by their prey affects the hunting behaviour of cephalopods and fish predators, J. Zool. **172**, 549 (1974).

[3] M. Milinski and R. Heller, Influence of a predator on the optimal foraging behaviour of sticklebacks (*Gasterosteus aculeatus* L.), Nature (London) **275**, 642 (1978).

[4] T. Caraco, S. Martindale, and H. R. Pulliam, Avian flocking in the presence of a predator, Nature (London) **285**, 400 (1980).

[5] F. Heppner, Three-dimensional structure and dynamics of bird flocks, in *Animal Groups in Three Dimensions*, edited by J. K. Parrish and W. M. Hamner (Cambridge University Press, Cambridge, 1997), p. 68.

[6] T. C. Michaelsen and I. Byrkjedal, 'Magic carpet' flight in shorebirds attacked by raptors on a migrational stopover site, Ardea **90**, 167 (2002).

[7] E. Bonabeau, M. Dorigo, and G. Théraulaz, *Swarm Intelligence: From Natural to Artificial Systems* (Oxford University Press, Oxford, 1999).

[8] M. Dorigo, M. Birattari *et al.*, Swarm intelligence, Scholarpedia **2**, 1462 (2007).

[9] I. Couzin, Collective minds, Nature (London) **445**, 715 (2007).

[10] A. Cavagna, A. Cimarelli, I. Giardina, G. Parisi, R. Santagati, F. Stefanini, and M. Viale, Scale-free correlations in starling flocks, Proc. Natl. Acad. Sci. USA **107**, 11865 (2010).

[11] W. Bialek, A. Cavagna, I. Giardina, T. Mora, O. Pohl, E. Silvestri, M. Viale, and A. M. Walczak, Social interactions dominate speed control in poising natural flocks near criticality, Proc. Natl. Acad. Sci. USA **111**, 7212 (2014).

[12] F. Vanni, M. Luković, and P. Grigolini, Criticality and Transmission of Information in a Swarm of Cooperative Units, Phys. Rev. Lett. USA **107**, 078103 (2011).

[13] A. Attanasi, A. Cavagna, L. Del Castello, I. Giardina, A. Jelic, S. Melillo, L. Parisi, O. Pohl, E. Shen, and M. Viale, Emergence of collective changes in travel direction of starling flocks from individual birds' fluctuations, J. R. Soc., Interface **12**, 20150319 (2015).

[14] N. Bain and D. Bartolo, Dynamic response and hydrodynamics of polarized crowds, Science **363**, 46 (2019).

[15] J. E. Treherne and W. A. Foster, Group transmission of predator avoidance behaviour in a marine insect: The Trafalgar effect, Anim. Behav. **29**, 911 (1981).

[16] T. Caro, *Antipredator Defenses in Birds and Mammals* (University of Chicago Press, Chicago, 2005).

[17] I. D. Chase, Models of hierarchy formation in animal societies, Behav. Sci. **19**, 374 (1974).

[18] M. Nagy, Z. Ákos, D. Biro, and T. Vicsek, Hierarchical group dynamics in pigeon flocks, Nature (London) **464**, 890 (2010).

[19] J. Shen, Cucker–Smale flocking under hierarchical leadership, SIAM J. Appl. Math. **68**, 694 (2008).

[20] B. Balázs, G. Vásárhelyi, and T. Vicsek, Adaptive leadership overcomes persistence–responsivity trade-off in flocking, J. R. Soc. Interface **17**, 20190853 (2020).

[21] J. E. Herbert-Read, J. Buhl, F. Hu, A. J. Ward, and D. J. Sumpter, Initiation and spread of escape waves within animal groups, R. Soc. Open Sci. **2**, 140355 (2015).

[22] A. Procaccini, A. Orlandi, A. Cavagna, I. Giardina, F. Zoratto, D. Santucci, F. Chiarotti, C. K. Hemelrijk, E. Alleva, G. Parisi *et al.*, Propagating waves in starling, *Sturnus vulgaris*, flocks under predation, Anim. Behav. **82**, 759 (2011).

[23] H.-P. Zhang, A. Be'er, E.-L. Florin, and H. L. Swinney, Collective motion and density fluctuations in bacterial colonies, Proc. Natl. Acad. Sci. USA **107**, 13626 (2010).

[24] E. Ben-Jacob, O. Schochet, A. Tenenbaum, I. Cohen, A. Czirok, and T. Vicsek, Generic modelling of cooperative growth patterns in bacterial colonies, Nature (London) **368**, 46 (1994).

[25] A. Cavagna, I. Giardina, and T. S. Grigera, The physics of flocking: Correlation as a compass from experiments to theory, Phys. Rep. **728**, 1 (2018).

[26] G. Gompper, R. G. Winkler, T. Speck, A. Solon, C. Nardini, F. Peruani, H. Löwen, R. Golestanian, U. B. Kaupp, L. Alvarez *et al.*, The 2020 motile active matter roadmap, J. Phys.: Condens. Matter **32**, 193001 (2020).

[27] C. Bechinger, R. Di Leonardo, H. Löwen, C. Reichhardt, G. Volpe, and G. Volpe, Active particles in complex and crowded environments, Rev. Mod. Phys. **88**, 045006 (2016).

[28] S. Ramaswamy, The mechanics and statistics of active matter, Annu. Rev. Condens. Matter Phys. **1**, 323 (2010).

[29] M. E. Cates and J. Tailleur, Motility-induced phase separation, Annu. Rev. Condens. Matter Phys. **6**, 219 (2015).

[30] M. F. Hagan and A. Baskaran, Emergent self-organization in active materials, Curr. Opin. Cell Biol. **38**, 74 (2016).

[31] T. Bäuerle, A. Fischer, T. Speck, and C. Bechinger, Self-organization of active particles by quorum sensing rules, Nat. Commun. **9**, 3232 (2018).

[32] F. D. C. Farrell, M. C. Marchetti, D. Marenduzzo, and J. Tailleur, Pattern Formation in Self-Propelled Particles with Density-Dependent Motility, Phys. Rev. Lett. **108**, 248101 (2012).

[33] A. P. Solon, J.-B. Caussin, D. Bartolo, H. Chaté, and J. Tailleur, Pattern formation in flocking models: A hydrodynamic description, Phys. Rev. E **92**, 062111 (2015).

[34] M. Brambilla, E. Ferrante, M. Birattari, and M. Dorigo, Swarm robotics: A review from the swarm engineering perspective, Swarm Intell. **7**, 1 (2013).

[35] F. J. Vernerey, E. Benet, L. Blue, A. Fajrial, S. L. Sridhar, J. Lum, G. Shakya, K. Song, A. Thomas, and M. Borden, Biological active matter aggregates: Inspiration for smart colloidal materials, Adv. Colloid Interface Sci. **263**, 38 (2019).

[36] U. Khadka, V. Holubec, H. Yang, and F. Cichos, Active particles bound by information flows, Nat. Commun. **9**, 3864 (2018).

[37] S. Muiños-Landin, A. Fischer, V. Holubec, and F. Cichos, Reinforcement learning with artificial microswimmers, Sci. Robot. **6**, eabd9285 (2021).

[38] D. Geiss, K. Kroy, and V. Holubec, Brownian molecules formed by delayed harmonic interactions, New J. Phys. **21**, 093014 (2019).

[39] J. Foss, A. Longtin, B. Mensour, and J. Milton, Multistability and Delayed Recurrent Loops, Phys. Rev. Lett. **76**, 708 (1996).

[40] H. Wernecke, B. Sándor, and C. Gros, Chaos in time delay systems, an educational review, Phys. Rep. **824**, 1 (2019).

[41] F. M. Atay, *Complex Time-Delay Systems: Theory and Applications* (Springer, Heidelberg, 2010).

[42] K. Pyragas, Control of chaos via extended delay feedback, Phys. Lett. A **206**, 323 (1995).

[43] P. Yang, R. A. Freeman, and K. M. Lynch, Optimal information propagation in sensor networks, in *Proceedings of the 2006 IEEE International Conference on Robotics and Automation, ICRA 2006* (IEEE Press, New York, 2006), pp. 3122–3127.

[44] F. Yin, X. Shao, M. Ji, and J. Wu, Quantifying the influence of delay in opinion transmission of COVID-19 information propagation: Modeling study, J. Med. Internet Res. **23**, e25734 (2021).

[45] C. Decker and R. Wattenhofer, Information propagation in the Bitcoin network, in *Proceedings of the IEEE P2P 2013* (IEEE, New York, 2013), pp. 1–10.

[46] E. Baccelli, P. Jacquet, B. Mans, and G. Rodolakis, Highway vehicular delay tolerant networks: Information propagation speed properties, IEEE Trans. Inf. Theory **58**, 1743 (2012).

[47] E. Forgoston and I. B. Schwartz, Delay-induced instabilities in self-propelling swarms, Phys. Rev. E **77**, 035203(R) (2008).

[48] L. Mier-y-Teran-Romero, E. Forgoston, and I. B. Schwartz, Coherent pattern prediction in swarms of delay-coupled agents, IEEE Trans. Rob. **28**, 1034 (2012).

[49] R. Piwowarczyk, M. Selin, T. Ihle, and G. Volpe, Influence of sensorial delay on clustering and swarming, Phys. Rev. E **100**, 012607 (2019).

[50] V. Holubec, D. Geiss, S. A. M. Loos, K. Kroy, and F. Cichos, Finite-Size Scaling at the Edge of Disorder in a Time-Delay Vicsek Model, Phys. Rev. Lett. **127**, 258001 (2021).

[51] R. Erban, J. Haškovec, and Y. Sun, A Cucker–Smale model with noise and delay, SIAM J. Appl. Math. **76**, 1535 (2016).

[52] A. Attanasi, A. Cavagna, L. Del Castello, I. Giardina, T. S. Grigera, A. Jelić, S. Melillo, L. Parisi, O. Pohl, E. Shen *et al.*, Information transfer and behavioural inertia in starling flocks, Nat. Phys. **10**, 691 (2014).

[53] H. Löwen, Inertial effects of self-propelled particles: From active Brownian to active Langevin motion, J. Chem. Phys. **152**, 040901 (2020).

[54] A. Cavagna, D. Conti, C. Creato, L. Del Castello, I. Giardina, T. S. Grigera, S. Melillo, L. Parisi, and M. Viale, Dynamic scaling in natural swarms, Nat. Phys. **13**, 914 (2017).

[55] A. Cavagna, L. Del Castello, I. Giardina, T. Grigera, A. Jelic, S. Melillo, T. Mora, L. Parisi, E. Silvestri, M. Viale *et al.*, Flocking and turning: A new model for self-organized collective motion, J. Stat. Phys. **158**, 601 (2015).

[56] D. Geiß, K. Kroy, and V. Holubec, Information conduction and convection in noiseless Vicsek flocks, Phys. Rev. E **106**, 014609 (2022).

[57] H. Chaté, F. Ginelli, G. Grégoire, and F. Raynaud, Collective motion of self-propelled particles interacting without cohesion, Phys. Rev. E **77**, 046113 (2008).

[58] D. J. G. Pearce and L. Giomi, Linear response to leadership, effective temperature, and decision making in flocks, Phys. Rev. E **94**, 022612 (2016).

[59] T. Vicsek, A. Czirók, E. Ben-Jacob, I. Cohen, and O. Shochet, Novel Type of Phase Transition in a System of Self-Driven Particles, Phys. Rev. Lett. **75**, 1226 (1995).

[60] H. Chaté, F. Ginelli, G. Grégoire, F. Peruani, and F. Raynaud, Modeling collective motion: Variations on the Vicsek model, Eur. Phys. J. B **64**, 451 (2008).

[61] J. M. Kosterlitz, The critical properties of the two-dimensional XY model, J. Phys. C **7**, 1046 (1974).

[62] M. Ballerini, N. Cabibbo, R. Candelier, A. Cavagna, E. Cisbani, I. Giardina, V. Lecomte, A. Orlandi, G. Parisi, A. Procaccini *et al.*, Interaction ruling animal collective behavior depends on topological rather than metric distance: Evidence from a field study, Proc. Natl. Acad. Sci. USA **105**, 1232 (2008).

[63] F. Ginelli, The physics of the Vicsek model, Eur. Phys. J.: Spec. Top. **225**, 2099 (2016).

[64] A. Cavagna, L. Di Carlo, I. Giardina, T. S. Grigera, and G. Pisegna, Equilibrium to off-equilibrium crossover in homogeneous active matter, Phys. Rev. Res. **3**, 013210 (2021).

[65] H. Pomeroy and F. Heppner, Structure of turning in airborne rock dove (*Columba livia*) flocks, The Auk **109**, 256 (1992).

[66] J. Brown, T. Bossomaier, and L. Barnett, Information flow in finite flocks, Sci. Rep. **10**, 3837 (2020).

[67] A. Cavagna, P. M. Chaikin, D. Levine, S. Martiniani, A. Puglisi, and M. Viale, Vicsek model by time-interlaced compression: A dynamical computable information density, Phys. Rev. E **103**, 062141 (2021).

[68] C. E. Shannon, A mathematical theory of communication, Bell System Tech. J. **27**, 379 (1948).

[69] T. M. Cover, *Elements of Information Theory* (John Wiley & Sons, Hoboken, New Jersey, 1999).

[70] A. Cavagna, D. Conti, I. Giardina, T. S. Grigera, S. Melillo, and M. Viale, Spatio-temporal correlations in models of collective motion ruled by different dynamical laws, Phys. Biol. **13**, 065001 (2016).

[71] A. Cavagna, I. Giardina, T. S. Grigera, A. Jelic, D. Levine, S. Ramaswamy, and M. Viale, Silent Flocks: Constraints on Signal Propagation across Biological Groups, Phys. Rev. Lett. **114**, 218101 (2015).

[72] R. Zwanzig, *Nonequilibrium Statistical Mechanics* (Oxford University Press, Oxford, 2001).

[73] M. Baiesi, C. Maes, and B. Wynants, Fluctuations and Response of Nonequilibrium States, Phys. Rev. Lett. **103**, 010602 (2009).

[74] U. Seifert and T. Speck, Fluctuation-dissipation theorem in nonequilibrium steady states, Europhys. Lett. **89**, 10007 (2010).

[75] B. Altaner, M. Polettini, and M. Esposito, Fluctuation-Dissipation Relations Far from Equilibrium, Phys. Rev. Lett. **117**, 180601 (2016).

[76] G. Jung and F. Schmid, Fluctuation-dissipation relations far from equilibrium: A case study, Soft Matter **17**, 6413 (2021).

[77] S. A. M. Loos, S. Hermann, and S. H. L. Klapp, Medium entropy reduction and instability in stochastic systems with distributed delay, Entropy **23**, 696 (2021).

[78] R. Olinky and L. Stone, Unexpected epidemic thresholds in heterogeneous networks: The role of disease transmission, Phys. Rev. E **70**, 030902(R) (2004).

[79] L. A. Meyers, B. Pourbohloul, M. E. Newman, D. M. Skowronski, and R. C. Brunham, Network theory and SARS: Predicting outbreak diversity, J. Theor. Biol. **232**, 71 (2005).

[80] G. Großmann, M. Backenköhler, and V. Wolf, Heterogeneity matters Contact structure and individual variation shape epidemic dynamics, PLoS ONE **16**, e0250050 (2021).